Separation and Purification Technology 203 (2018) 41–47

Contents lists available at ScienceDirect

Separation and Purification Technology

journal homepage: www.elsevier.com/locate/seppur

Unravelling the transport mechanism of pore-filled membranes for hydrogen separation

Alba Arratibel[a,b], D. Alfredo Pacheco Tanaka[b], Thomas J.A. Slater[c], Timothy L. Burnett[c], Martin van Sint Annaland[a], Fausto Gallucci[a,*]

[a] Chemical Process Intensification, Department of Chemical Engineering and Chemistry, Eindhoven University of Technology (TU/e), Den Dolech 2, 5612AD Eindhoven, The Netherlands
[b] TECNALIA, Energy and Environment Division, Mikeletegi Pasealekua 2, 20009 San Sebastian-Donostia, Spain
[c] Henry Moseley X-ray Imaging Facility, School of Materials, University of Manchester, M13 9PL, United Kingdom

ARTICLE INFO

Keywords:
Hydrogen separation
Membrane preparation
Pore-filled membranes

ABSTRACT

The permeation characteristics of palladium pore filled (PF) membranes have been investigated with gas permeation and structural characterization of the membranes. PF membranes have been prepared by filling with Pd the nanoporous γ-Al_2O_3/YSZ (or pure YSZ) layer supported onto porous α-Al_2O_3 and ZrO_2. The number of nanoporous layers and the applied vacuum level during the electroless plating process have been studied. Gas permeation properties of the PF membranes have been determined in a temperature range of 300–550 °C. The measured hydrogen permeances have been found to be lower than previously reported for similar membranes. It has been found that the hydrogen fluxes do not depend on the thickness of the nanoporous layers (γ-Al_2O_3/YSZ or pure YSZ) or on the vacuum pump employed for filling with Pd. The physicochemical characterization performed showed that the palladium deposited does not form a percolated network across the mesoporous layer(s), leading to low hydrogen permeances and thus low H_2/N_2 perm-selectivities.

1. Introduction

Several reports on the use of Pd-based membranes for hydrogen separation in fluidized bed membrane reactors have been published in the last few years [1–5]. When particles are in continuous contact with the (thin) hydrogen selective layer, depending on the gas velocity, particles can erode the membrane surface by creating pinholes, leading to a decrease in the membrane perm-selectivity.

The pore-filled (PF) type membranes avoid direct contact of fluidized particles with the hydrogen selective material, since the Pd is located inside the nano-pores of the substrate [6,7], protected by a mesoporous layer composed of γ-Al_2O_3/YSZ or pure YSZ. Another advantage of this membrane configuration is that the embrittlement due to α-β phase transition is prevented due to the nanometric size of the palladium clusters, where the hydrogen loading preferentially occurs on the surface rather than on the interior of the particles [8].

It has been reported that, when Pd is filled in the nanopores composed of only γ-Al_2O_3 the membranes are not stable at temperatures above 400 °C due to the large difference in the thermal expansion coefficient of Pd and alumina; in addition, the hydrogen permeance of conventional Pd alloy membranes supported on alumina showed a decay when they were exposed to hydrogen at high temperature (650 °C) [9]. Inclusion of YSZ into the mesoporous layer diminishes the probability of alloying of Pd with alumina, while the thermal expansion is closer to that of palladium [10]. For these reasons, in a previous paper [7] the study was focused on the preparation of Pd PF membranes with a nanoporous layer made out of γ-Al_2O_3/YSZ with more than 50 wt% of YSZ. The permeation performance of this PF membrane was studied in the temperature range of 500–550 °C and the ideal H_2/N_2 perm-selectivity was around 50. The ideal perm-selectivity is defined as the radio of the permeability of two gas species, $\alpha_{ab} = Pe_{(a)}/Pe_{(b)}$, measured separately under same conditions. This low value was attributed to the low hydrogen flux through the membrane. The aim of the present work is to extend the study on PF membranes and understand the reason for the very low permeation rates observed in the previous work.

In the present work, the permeation properties of pore-filled membranes have been studied by varying the porous support material, thickness and composition of the nanoporous layers and the vacuum level applied during VA-ELP (vacuum-assisted electroless plating), among other parameters. Physicochemical characterization has been performed on the nanoporous layers containing a different YSZ content

* Corresponding author.
E-mail address: F.Gallucci@tue.nl (F. Gallucci).

https://doi.org/10.1016/j.seppur.2018.04.016
Received 9 March 2018; Received in revised form 3 April 2018; Accepted 4 April 2018
Available online 05 April 2018

and calcined at 550 °C or 650 °C.

2. Experimental

2.1. Membrane preparation

The γ-Al_2O_3/YSZ layers were deposited onto porous α-Al_2O_3 (OD/ID 10/7 and 10/4 mm) with a pore size of 100 nm, provided by Rauschert Kloster Veilsdorf, according to the procedure reported in a previous work [7]. Calcination of the deposited layers was carried out at 550 °C or 650 °C, which allows studying the effect of the pore-size of the layer on the membrane performance. Then the support is activated with nano-palladium nuclei and another porous layer (the so-called protective layer) was deposited, as reported previously. Afterward, the nano-palladium particles in the first mesoporous layer were forced to grow by vacuum-assisted electroless plating using a rotatory (Edwards RV3) and a turbomolecular pump (Edwards T-Station 75), where the maximum vacuum measured was $2{\cdot}10^{-2}$ mbar and $1{\cdot}10^{-6}$ mbar, respectively. Finally, the membrane was annealed at 550 °C for 4 h under 10 vol.% H_2/90 vol.% N_2. The VA-ELP and annealing processes were repeated until the nitrogen leakage at room temperature of the membrane was below $8{\cdot}10^{-9}$ mol m^{-2} s^{-1} Pa^{-1} (this value is considered as the maximum acceptable value for preparing a good membrane).

The nanoporous layer was also deposited onto porous supports composed of asymmetric α-Al_2O_3 (OD/ID 10/7 mm) with an intermediate TiO_2 layer and a ZrO_2 top layer with 3 nm pore size (see Fig. 1). In this case, the top porous support layer was first activated with palladium nuclei and then a protective layer of YSZ was deposited, which is possible owing to the similar thermal expansion coefficient with the top layer of the support (ZrO_2). Then, Pd nano-seeds were forced to grow by VA-ELP as in the case of the α-Al_2O_3 support, followed by the annealing process. As described for α-Al_2O_3 supports, the cycle (VA-ELP and annealing process) was repeated until the nitrogen permeance was below $8{\cdot}10^{-9}$ mol m^{-2} s^{-1} Pa^{-1}.

Various vacuum levels were applied during the vacuum-assisted electroless plating (VA-ELP) step. A vacuum is applied at the inner side of the tubes in order to force the Pd^{2+} ions present in the plating solution to pass through the pores; therefore, the plating will be carried out inside the pores where Pd (catalyst for the reaction) is present. As the vacuum level increased, the number of cycles (VA-ELP and annealing) needed to fill the pores decreased (see Table 1), so that the plating time can be increased while still avoiding growth of palladium on the surface.

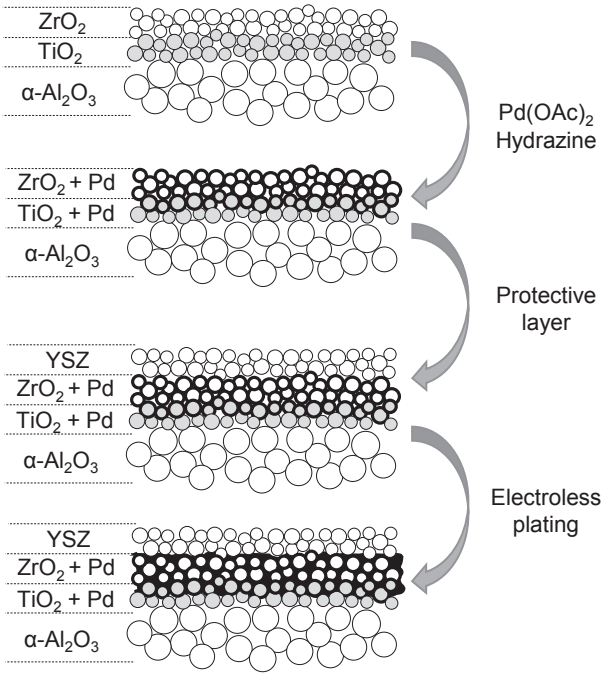

Fig. 1. Schematic representation of the preparation of Pd pore-filled membranes using porous α-Al_2O_3 support with an intermediate TiO_2 layer and a ZrO_2 top layer with a pore size of 3 nm.

Table 1
Capabilities of the vacuum pump during VA-ELP of pore-filled membranes.

Parameter	Rotatory pump	Turbomolecular pump
Measured pressure during ELP (mbar)	$2{\cdot}10^{-2}$	$1{\cdot}10^{-6}$
Number of VA-ELP	4–15	2–6
Plating time (min)	4–12	8–60

2.2. Gas permeation measurements

The membranes have been tested with pure gases (hydrogen and nitrogen) in an empty reactor in the temperature range of 300–550 °C and with a transmembrane pressure difference of 30–400 kPa. The setup used for single gas measurements was described in our previous work [7]. The pressure difference between retentate and permeated side (at atmospheric pressure) was regulated by a back-pressure regulator (Horiba Stec. UR-7340 model) at the retentate side. Permeated fluxes were measured with an automated soap film flow meter (Horiba STEC VP-1, VP-2 and VP-3).

2.3. Characterization

The pore size and surface area of the mesoporous materials calcined at different temperatures were obtained from the BET nitrogen adsorption isotherm obtained with a Thermo Scientific Surfer. The crystal structure of γ-Al_2O_3/YSZ powders was obtained by powder X-ray diffraction (Rigaku MiniFlex 600) in the 2θ range of 20–90° with a step size of 0.02° 2θ, operating at 40 kV and 15 mA with Cu-Kα radiation. The crystallite size was calculated using the Scherrer equation. The carbon content has been determined by the infrared absorption method after combustion in an induction furnace using a CS400 LECO analyzer, where the produced CO_2 volume was measured. The membrane thickness was measured using cross-sectional images with a SEM (FEI Quanta 250 FEG).

Preparation of a sample for the transmission electron microscope (TEM) was undertaken using a Thermo Scientific Helios 660 focused ion beam (FIB) dual-beam instrument. A cross-sectional sample was taken from the surface of a cut sample, using a 30 kV Ga ion beam to prepare an approximately 150 nm thick lamella.

Characterization of the Pd distribution was carried out with a Thermo Scientific Talos F200A scanning transmission electron microscope (STEM), possessing a high brightness X-FEG electron source and Super-X energy dispersive X-ray (EDX) silicon drift detectors (SDDs). The microscope was operated at an accelerating voltage of 200 kV with a beam current of 260 pA, a convergence angle of 12 mrad and a HAADF acceptance inner angle of 50 mrad. EDX spectrum images were acquired with the Thermo Scientific Velox software (version 1.6.0), with a total per pixel dwell time of approximately 2.5 ms and an image size of 387 × 439 pixels. A tilt series for HAADF-STEM tomography was acquired using Xplore3D acquisition software at angular increments of 1° from −75° to +75°. Image alignment was performed using patch tracking in the IMOD software package, followed by the use of a simultaneous reconstruction technique (SIRT) to perform the reconstruction with 20 iterations. Segmentation of Au and Pd voxels was performed using an auto threshold in Avizo. Visualization of the 3D reconstructions was also performed in the Avizo software package.

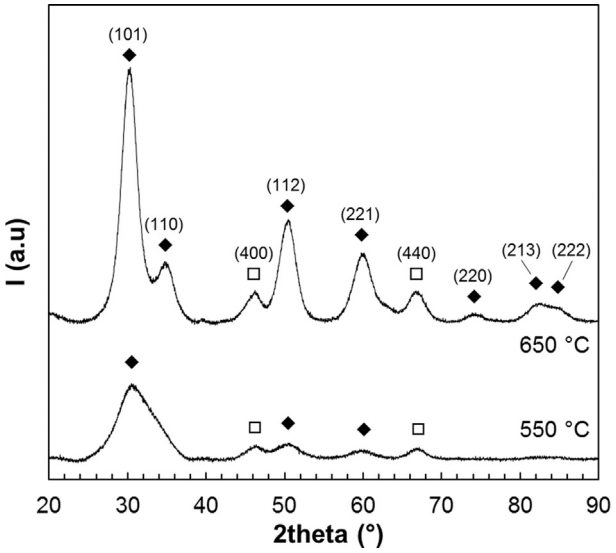

Fig. 2. XRD patterns of YSZ-γ-Al_2O_3 powders (50 wt% YSZ) calcined in air at 550 °C and 650 °C for 3 h. (♦): $(ZrO_2)_{0.92}(Y_2O_3)_{0.08}$ (JCPDS 01-070-4431); (□) Gamma-Al_2O_3 (JCPDS 00–002-1420).

3. Results and discussion

3.1. Characterization of mesoporous powders

According to the XRD patterns for samples (50 wt% YSZ/50 wt% γ-Al_2O_3) calcined at 550 °C or 650 °C, shown in Fig. 2, the peaks related to cubic YSZ become more intense and sharp when the calcination was carried out at 650 °C due to the crystal growth. It was calculated that the crystal size of YSZ increases from 1.7 nm to 3.5 nm as the calcination temperature increased from 550 °C to 650 °C. Peaks centered at ~45° and ~67° are related to amorphous γ-Al_2O_3 [11] and became also more intense when the sample was calcined at 650 °C.

The nitrogen adsorption/desorption isotherm of YSZ/γ-Al_2O_3 (50/50 wt%) samples calcined at 550 °C and 650 °C are shown in Fig. 3 (left). The isotherm profiles present a type IV shape according to IUPAC classification with a recognizable hysteresis loop typical for mesoporous materials [12]. The surface area decreased from 300 to 257 m^2 g^{-1} as the calcination temperature was increased from 550 °C to 650 °C, both presenting similar pore size distributions (see Fig. 3, right).

3.2. Membrane characterization

3.2.1. Nanoporous membrane

The thickness of the supported nanoporous membranes prepared with just the protective layer, and membranes with three mesoporous layers (the first two layers with palladium seeding and the third one as a protective layer), have been characterized with cross-section SEM (see Fig. 4). Table 2 summarizes the configuration and thickness of some nanoporous membranes that have been prepared with different support materials (α-Al_2O_3 and ZrO_2). As was explained in our previous study [7], relatively thick (> 3 μm) γ-Al_2O_3/YSZ nanoporous layers that possess a high content of YSZ but without cracks are very difficult to obtain. Therefore, for layers with a high YSZ content, thinner membranes should be prepared. For this reason, the thickness of a single layer made of pure YSZ (PF-Z2) was only 0.31 μm, while membranes with three layers made by 50 wt% YSZ possess thicker layers (2.47–3.27 μm). The difference in thickness of samples with three layers could be related to a non-uniform layer formed during the drying process. The tubes have to turn horizontally in order to get a homogenous layer. A small curvature in the support (junction between porous and dense ceramic tubes [7]) can leads to a thickness deviation.

Pacheco Tanaka et al. reported the preparation of PF Pd membranes in a γ-Al_2O_3/YSZ (50 wt% YSZ) nanoporous layer supported using symmetric alumina capillary tubes (OD: 2 mm) with 150 nm pore size; using this support, a 3 μm thick γ-Al_2O_3/YSZ layer was obtained in only one dipping calcination process [6]. In the current study, asymmetric alumina tubes were used and several attempts were carried out to prepare γ-Al_2O_3/YSZ layers with a similar thickness to those reported by Pacheco Tanaka without defects, however, without success. This indicates the importance of the support in the preparation of the Pd pore-filled membranes.

3.2.2. Pd pore-filled membranes

The nitrogen permeation of the PF-membranes has been measured at room temperature after each VA-ELP and annealing step. The gas permeation properties (H_2 and N_2) of the PF-membranes with a nitrogen permeance lower than $8{\cdot}10^{-9}$ mol m^{-2} s^{-1} Pa^{-1} at room temperature were tested in the temperature range of 300–550 °C. In Table 3 the characteristics of the prepared membranes, their permeation properties and the number of VA-ELP cycles required to reach the desired maximum N_2 permeance are listed. Membranes prepared using α-Al_2O_3 as a support need a larger number of cycles when a rotatory pump was employed (from 8 to 12), while with turbomolecular pump lower nitrogen permeances was obtained with fewer cycles (from 2 to 6). Some membranes have been prepared using both types of pumps, where the required number of cycles was in between what was required when using the same pump (from 6 to 10). This is related to the suction

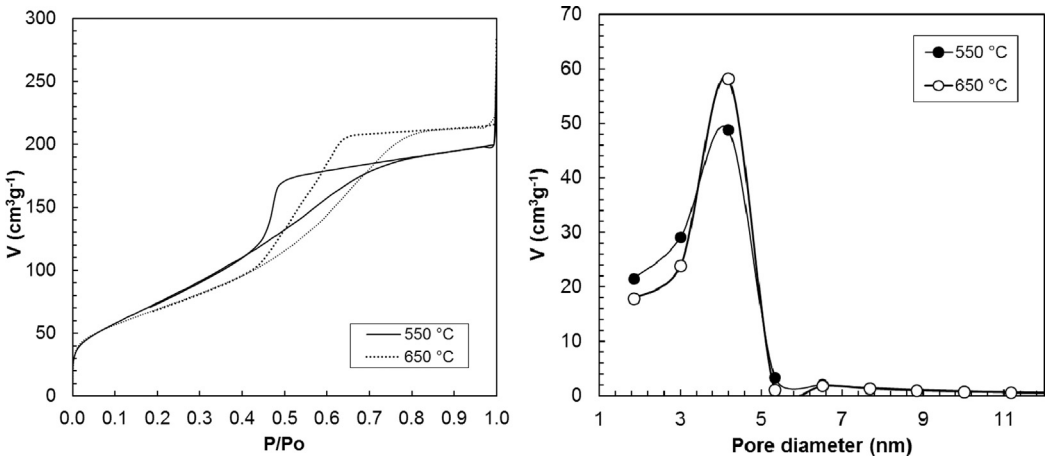

Fig. 3. Nitrogen isotherms and pore size distributions of YSZ/γ-Al_2O_3 powders (50 wt% YSZ) calcined in air at 550 °C and 650 °C for 3 h.

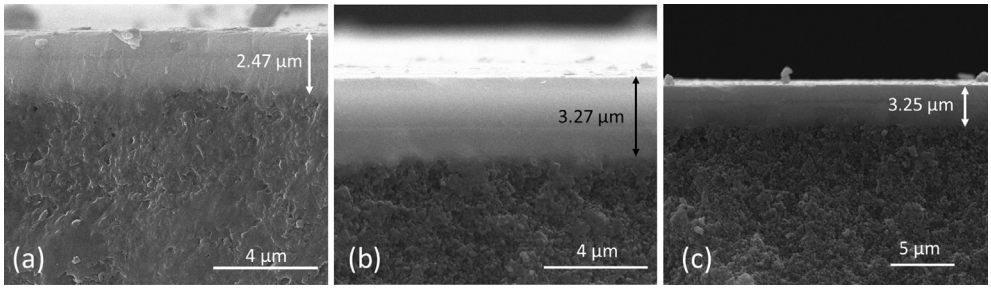

Fig. 4. SEM cross section images of PF-A133 (a), PF-145 (b) and PF-155 (c).

Table 2
γ-Al_2O_3/YSZ nanoporous layers prepared on α-alumina (100 nm pore size) and zirconia (3 nm pore size) supports.

Membrane	Mesoporous layer(s)			
	Number of layers[a]	YSZ content (wt.%)	Calcination temperature (°C)	Thickness (µm)
PF-A45	2	60	550	2.04 ± 0.10
PF-A133	3	50	550	2.47 ± 0.12
PF-A145	3	50	550	3.27 ± 0.04
PF-A155	3	50	550	3.25 ± 0.12
PF-A172	3	50	550	2.94 ± 0.12
PF-Z2	1	100	550	0.31 ± 0.02

[a] Membranes with two or three layers means that one and two layers were prepared before seeding and then the protective layer was deposited. For membranes with one layer, the supports were seeded and the protective layer was deposited on top.

level of each pump. The turbomolecular pump allows performing the electroless plating for longer periods compared to the rotatory pump, while still avoiding the growth of palladium on the surface. On the other hand, the number of VA-ELP cycles does not depend on the number of mesoporous layers, composition or calcination temperature, as can be concluded from Table 3.

The measured hydrogen permeance and ideal H_2/N_2 perm-selectivity of the membranes summarized in Table 3 are also plotted in Fig. 5. It can be observed that the performance of the membranes is not directly related to the thickness of the mesoporous layers or the number

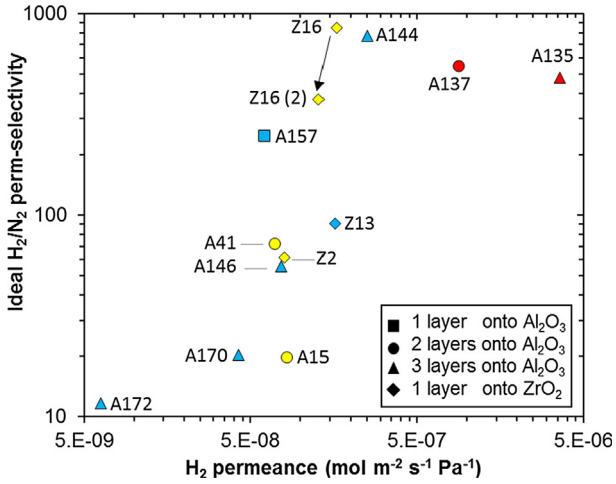

Fig. 5. Hydrogen permeance and ideal H_2/N_2 perm-selectivity of tested pore-filled membranes with different numbers of mesoporous layers and different support materials. Symbol colors refer to the testing temperature: 300 °C (blue), 400 °C (yellow) and 550 °C (red). (For interpretation of the references to colour in this figure legend, the reader is referred to the web version of this article.)

of platings performed before the permeation test. The best performance (in terms of hydrogen permeance) was obtained for a membrane prepared onto an Al_2O_3 support, viz. PF-A135, containing three mesoporous layers (where the third layer acts as a protective layer), with a hydrogen permeance of $\sim 3.6{\cdot}10^{-6}$ mol m^{-2} s^{-1} Pa^{-1} at 550 °C and an

Table 3
Summary of tested membranes with nitrogen permeance below $8{\cdot}10^{-9}$ mol m^{-2} s^{-1} Pa^{-1}.

Membrane	Support			Nano-porous layer(s)			VA-ELP		Permeation properties			
	Material	Pore size (nm)	OD/ID (mm)	Number of layers[a]	YSZ content (wt%)	Calcination temp. (°C)	Pump[b]	Number of cycles[c]	Temp. (°C)	ΔP (bar)	H_2 permeance (mol m^{-2} s^{-1} Pa^{-1})	H_2/N_2
PF-A15	α-Al_2O_3	100	10/7	2	60	550	R	8	400	1	$8.27{\cdot}10^{-8}$	20
PF-A41	α-Al_2O_3	100	10/7	2	50	550	R	7	400	1	$7.02{\cdot}10^{-8}$	72
PF-A45	α-Al_2O_3	100	10/7	2	60	550	R	9	400	1	$1.95{\cdot}10^{-7}$	27
PF-A135	α-Al_2O_3	100	10/7	3	50	650	R	8	550	0.3	$3.63{\cdot}10^{-6}$	478
PF-A137	α-Al_2O_3	100	10/7	2	50	550	R	12	550	1	$8.87{\cdot}10^{-7}$	552
PF-A144	α-Al_2O_3	100	10/7	3	50	550	R+T	6	300	1	$2.50{\cdot}10^{-7}$	777
PF-A146	α-Al_2O_3	100	10/7	3	50	550	R+T	10	550	3	$7.72{\cdot}10^{-8}$	56
PF-A157	α-Al_2O_3	100	10/7	1	50	550	T	6	300	3	$6.06{\cdot}10^{-8}$	246
PF-A170	α-Al_2O_3	100	10/4	3	50	550	T	4	300	1	$4.23{\cdot}10^{-8}$	20
PF-A172	α-Al_2O_3	100	10/4	3	50	550	T	2	300	2	$6.28{\cdot}10^{-9}$	12
PF-Z2	ZrO_2	3	10/7	1	100	650	R	15	400	1	$8.00{\cdot}10^{-8}$	62
PF-Z13	ZrO_2	3	10/7	1	100	650	R	4	300	1	$1.60{\cdot}10^{-7}$	90
PF-Z16	ZrO_2	3	10/7	1	100	650	R	4	400	1	$1.64{\cdot}10^{-7}$	850
PF-Z16 (2)[d]	ZrO_2	3	10/7	1	100	650	R	4	400	1	$1.29{\cdot}10^{-7}$	375

[a] Membranes with 2 and 3 layers means that 1 and 2 layers were prepared before seeded and then the protective layer was deposited. For membranes with one layers, the supports were seeded and the protective layers was deposited on top.
[b] R: Rotatory pump. T: turbomolecular pump.
[c] Each cycle is referred to the VA-ELP process and the annealing treatment.
[d] Permeation after keeping membrane Z16 under N_2 at 400 °C overnight.

ideal perm-selectivity of ~478. However, this value is too low for the implementation of these membranes for reactors/separators for hydrogen production with high purity. In addition, the number of VA-ELP steps performed to reach this selectivity (low N_2 leakage) was 8, which is not feasible for industrial scale production because of the thermal treatment (annealing) that has to be repeated after each VA-ELP step. Moreover, other membranes showed lower hydrogen permeances, reaching values around 10^{-8}–10^{-9} mol m^{-2} s^{-1} Pa^{-1}, which are much lower than those obtained by Pacheco Tanaka et al. [6,13].

For the case of ZrO_2 supports with a top layer pore size of 3 nm, a single mesoporous layer of pure YSZ was deposited thanks to the thermal stability of ZrO_2 and YSZ in the presence of H_2 at high temperature in comparison with alumina [9]. In this case, the membranes tested have been prepared using the rotatory pump (using 4 to 15 cycles). Membranes PF-Z2, PF-Z13 and PF-Z16 showed H_2 permeances around ~$1{\cdot}10^{-7}$ mol m^{-2} s^{-1} Pa^{-1} at 300–400 °C (see Table 3). The best results were observed for PF-Z16 with an ideal H_2/N_2 perm-selectivity of 850. However, after keeping the membrane under nitrogen overnight, the H_2 permeance decreased to 40% of the initial value, indicated in Fig. 5 as Z16(2). This decay is attributed to the presence of a TiO_2 layer between the ZrO_2 top layer and the α-Al_2O_3 of the support (see Fig. 1). During the preparation of the pore-filled membranes, palladium can come into contact with the TiO_2 and fill the pores of the TiO_2 layer. Strong interaction between Pd and TiO_2 was observed before by Fernandez et al. [3], when a conventional Pd-based membrane was brought into contact with TiO_2 particles during the water-gas-shift reaction in a fluidized bed Pd membrane reactor. Under H_2 and at high temperature in the presence of Pd, TiO_2 can be reduced to Ti metal, forming a Pd-Ti alloy with a low H_2 permeation [14].

In order to understand why the hydrogen flux is so low, the permeation properties of two membranes, PF-A137 and PF-A146, prepared with the rotary pump and both the rotatory and turbomolecular pumps respectively, have been measured as a function of the number of VA-ELP and annealing cycles. As shown in Fig. 6, after a number of cycles the N_2 and H_2 fluxes decrease. After several cycles, the nitrogen leakage decreases to $1{\cdot}10^{-9}$ mol m^{-2} s^{-1} Pa^{-1}, while the hydrogen permeation continues to decrease, resulting in ideal perm-selectivities of ~552 (PF-A137) and ~56 (PF-A146). Lower H_2 fluxes are expected if more cycles are repeated in order to decrease the N_2 flux. To answer why the hydrogen permeances are so low (in many cases even in the order of 10^{-8}–10^{-9} mol m^{-2} s^{-1} Pa^{-1} as shown in Table 3), a physicochemical characterization of the PF-membranes has been performed.

One reason for the low H_2 flux could be the formation of carbon (which blocks the hydrogen transport through the membrane) during the annealing process due to the chemicals employed during the preparation of the membranes. The carbon content of a membrane was investigated by carbon analysis undertaken by CO_2 infrared detection. The amount of carbon measured was 0.013 wt%, which is sufficiently low to exclude carbon formation as cause for the low H_2 permeance of the membranes.

The microstructure of the PF membranes has been characterized in more detail by TEM electron tomography. The three nano-porous layers deposited in the membrane PF-A172 have been observed by HAADF STEM (high-angle annular dark-field scanning transmission electron microscope) imaging (see Fig. 7a). According to STEM-EDX analysis, the top layer contains almost no Pd, which is expected in the protective layer as the Pd seeds were not deposited in this layer. The second layer contains a small number of discrete particles and the bottom layer contains a large number of discrete Pd particles (see Fig. 7b). There are interfaces of approximately 10–20 nm between each layer and the one between the second and bottom layers is rich in Pd, which is due to the presence of a higher concentration of Pd seeds in the pores of the interphases. The Al (Fig. 7c) and Zr (Fig. 7d) concentrations were approximately constant through the membrane. These results are fairly clear from the 2D images. In addition, the non-percolated palladium network along the mesoporous layers has been confirmed by STEM tomography (Fig. 8 and Supplementary Videos). The 3D reconstruction validates that although small clusters of Pd particles are interconnected at the interface between the two layers, they are in general discrete and do not form an interconnected network. However, the resolution of the STEM tomography in this case is approximately 5–10 nm and therefore it could be possible that the interconnections smaller than 5 nm are not resolved. Higher resolution imaging in 2D at thin regions of the sample confirms that the larger Pd nanoparticles are not connected and supports the tomography data (Supplementary Fig. S1). The results of STEM imaging suggests that hydrogen molecules need to split and recombine several times before passing through the membrane, thus resulting in a low hydrogen transport, much lower than expected.

The observed microstructure does not yet explain why the palladium grains do not grow in an interconnected structure. This require additional research efforts, as the PF membranes are still very interesting, considering that the amount of palladium used in the pore-filled membrane is a small fraction of that used for conventional supported membranes.

4. Conclusions

The permeation properties of several pore-filled membranes for hydrogen separation have been studied in detail in order to understand why the hydrogen flux and thus the ideal perm-selectivity are much lower than expected. Membranes with different support materials and different numbers of nanoporous layers have been prepared using different vacuum levels for the VA-ELP. It has been observed that the number of nanoporous layers and the applied vacuum level for ELP is not directly related to the permeation properties of the membranes. It has been concluded by electron tomography analysis that the main

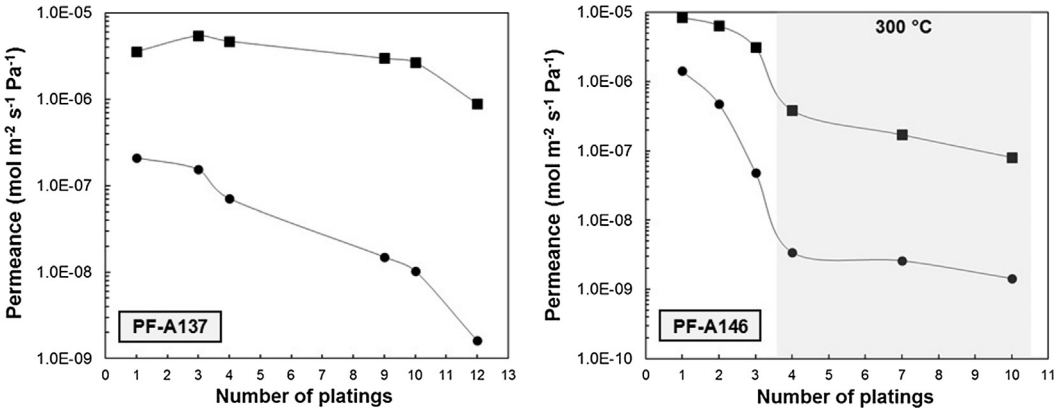

Fig. 6. H_2 (squares) and N_2 (circles) permeances of pore-filled membranes PF-A137 (left) and PF-A146 (right) measured at 550 °C.

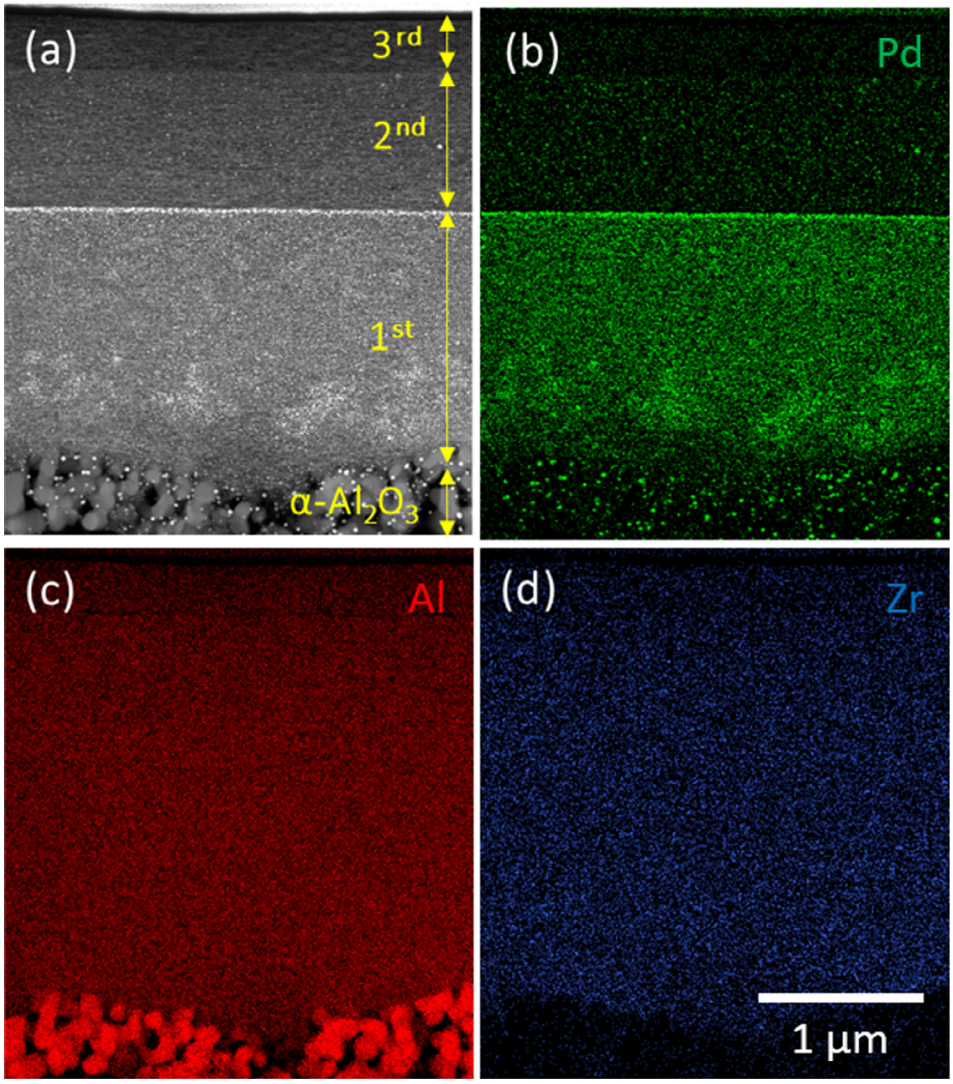

Fig. 7. HAADF STEM cross section image of PF-A172 (a) and STEM-EDX mapping of Pd (b), Al (c) and Zr (d).

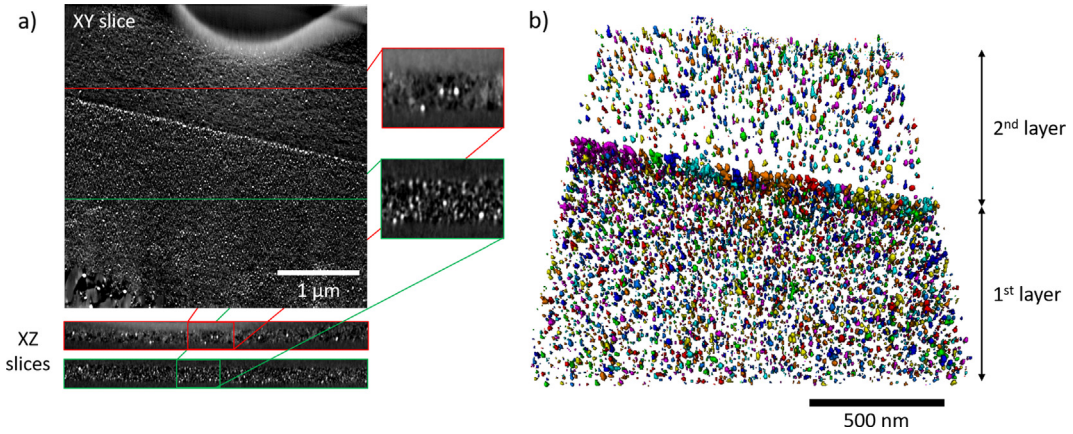

Fig. 8. A 3D reconstruction of Pd obtained by STEM tomography. (a) Slices through the reconstruction (in both the XY and XZ directions) showing the discrete nature of the Pd nanoparticles with magnified regions of the XZ slices. (b) Volume rendering of the segmented Pd nanoparticles.

reason for the low hydrogen flux through the membranes is that the Pd does not form an interconnected network across the mesoporous layers. Hence, the hydrogen needs to split and recombine several times along the palladium clusters created throughout the porous media. Further studies need to be carried out in order to understand why the palladium grains grow without connection to each other.

Acknowledgments

The presented work is funded within FERRET project as part of

European Union's Seventh Framework Programme (FP7/2007-2013) for the Fuel Cells and Hydrogen Joint Technology Initiative under grant agreement n° 621181. Note: "The present publication reflects only the authors' views and the Union is not liable for any use that may be made of the information contained therein". The Talos TEM was funded as part of HEFCE funding in the UK Research Partnership Investment Funding (UKRPIF) Manchester RPIF Round 2.

Appendix A. Supplementary material

Supplementary data associated with this article can be found, in the online version, at https://doi.org/10.1016/j.seppur.2018.04.016.

References

[1] A. Helmi, E. Fernandez, J. Melendez, D. Pacheco Tanaka, F. Gallucci, M. van Sint Annaland, Fluidized bed membrane reactors for ultra pure h2 production—a step forward towards commercialization, Molecules 21 (2016) 376, http://dx.doi.org/10.3390/molecules21030376.

[2] J.A. Medrano, E. Fernandez, J. Melendez, M. Parco, D.A.P. Tanaka, M. van Sint Annaland, F. Gallucci, Pd-based metallic supported membranes: High-temperature stability and fluidized bed reactor testing, Int. J. Hydrogen Energy. (2015) 1–13, http://dx.doi.org/10.1016/j.ijhydene.2015.10.094.

[3] E. Fernandez, A. Helmi, K. Coenen, J. Melendez, J.L. Viviente, D.A. Pacheco Tanaka, M. van Sint Annaland, F. Gallucci, Development of thin Pd–Ag supported membranes for fluidized bed membrane reactors including WGS related gases, Int. J. Hydrogen Energy. 40 (2015) 3506–3519.

[4] E. Fernandez, A. Helmi, J.A. Medrano, K. Coenen, A. Arratibel, J. Melendez, N.C.A. de Nooijer, V. Spallina, J.L. Viviente, J. Zuñiga, M. van Sint Annaland, D.A. Pacheco Tanaka, F. Gallucci, Palladium based membranes and membrane reactors for hydrogen production and purification: An overview of research activities at Tecnalia and TU/e, Int. J. Hydrogen Energy. 42 (2017) 13763–13776, http://dx.doi.org/10.1016/j.ijhydene.2017.03.067.

[5] E. Fernandez, K. Coenen, A. Helmi, J. Melendez, J. Zuñiga, D.A. Pacheco Tanaka, M. Van Sint Annaland, F. Gallucci, Preparation and characterization of thin-film Pd-Ag supported membranes for high-temperature applications, Int. J. Hydrogen Energy. 40 (2015) 13463–13478, http://dx.doi.org/10.1016/j.ijhydene.2015.08.050.

[6] D.A. Pacheco Tanaka, M.A. Llosa Tanco, J. Okazaki, Y. Wakui, F. Mizukami, T.M. Suzuki, Preparation of "pore-fill" type Pd–YSZ–γ-Al2O3 composite membrane supported on α-Al2O3 tube for hydrogen separation, J. Memb. Sci. 320 (2008) 436–441, http://dx.doi.org/10.1016/j.memsci.2008.04.044.

[7] A. Arratibel, U. Astobieta, D.A. Pacheco Tanaka, M. van Sint Annaland, F. Gallucci, N2, He and CO_2 diffusion mechanism through nanoporous YSZ/γ-Al2O3 layers and their use in a pore-filled membrane for hydrogen membrane reactors, Int. J. Hydrogen Energy. 41 (2016) 8732–8744.

[8] R.J. Wolf, M.W. Lee, J.R. Ray, Pressure-composition isotherms for nanocrystalline palladium hydride, Phys. Rev. Lett. 73 (1994) 557–562.

[9] J. Okazaki, T. Ikeda, D.A. Pacheco Tanaka, M.A. Llosa Tanco, Y. Wakui, K. Sato, F. Mizukami, T.M. Suzuki, Importance of the support material in thin palladium composite membranes for steady hydrogen permeation at elevated temperatures, Phys. Chem. Chem. Phys. 11 (2009) 8632–8638, http://dx.doi.org/10.1039/b909401f.

[10] S. Tekeli, Influence of alumina addition on grain growth and room temperature mechanical properties of 8YSCZ/Al2O3 composites, Compos. Sci. Technol. 65 (2005) 967–972, http://dx.doi.org/10.1016/j.compscitech.2004.10.024.

[11] M.I.F. Macedo, C.C. Osawa, C.A. Bertran, Sol-gel synthesis of transparent alumina gel and pure gamma alumina by urea hydrolysis of aluminum nitrate, J. Sol-Gel Sci. Technol. 30 (2004) 135–140.

[12] K.S.W. Sing, D.H. Everett, R.A.W. Haul, L. Moscou, R.A. Pierotti, J. Rouquérol, T. Siemieniewska, Reporting physisortion data for gas/solid systems, Pure Appl. Chem. 57 (1985) 603–619.

[13] D.A. Pacheco Tanaka, M.A. Tanco Llosa, T. Nagase, J. Okazaki, Y. Wakui, F. Mizukami, T.M. Suzuki, Fabrication of hydrogen-permeable composite membranes packed with palladium nanoparticles, Adv. Mater. 18 (2006) 630–632, http://dx.doi.org/10.1002/adma.200501900.

[14] Y. Huang, R. Dittmeyer, Preparation and characterization of composite palladium membranes on sinter-metal supports with a ceramic barrier against intermetallic diffusion, J. Memb. Sci. 282 (2006) 296–310, http://dx.doi.org/10.1016/j.memsci.2006.05.032.